SUPPORTING INFORMATION FOR:

Polaronic transport and current blockades in epitaxial silicide nanowires and nanowire arrays

Violeta Iancu,[†,‖] X.-G. Zhang,[‡,⊥] Tae-Hwan Kim,[‡,#] Laurent D. Menard,[¶] P. R. C. Kent,[§] Michael E. Woodson,[¶] J. Michael Ramsey,[¶] An-Ping Li,[‡] and Hanno H. Weitering[*,†,@]

Department of Physics and Astronomy, The University of Tennessee, Knoxville, TN 37966, USA, Center for Nanophase Materials Sciences, Oak Ridge National Laboratory, Oak Ridge, TN 37831, USA, Department of Chemistry, University of North Carolina, Chapel Hill, NC 27599, USA , and Center for Nanophase Materials Sciences and Computer Science and Mathematics Division, Oak Ridge National Laboratory, Oak Ridge, TN 37831

E-mail: hanno@utk.edu

[*]To whom correspondence should be addressed

[†]Department of Physics and Astronomy, The University of Tennessee, Knoxville, TN 37966, USA

[‡]Center for Nanophase Materials Sciences, Oak Ridge National Laboratory, Oak Ridge, TN 37831, USA

[¶]Department of Chemistry, University of North Carolina, Chapel Hill, NC 27599, USA

[§]Center for Nanophase Materials Sciences and Computer Science and Mathematics Division, Oak Ridge National Laboratory, Oak Ridge, TN 37831

[‖]Current address: Laboratory of Solid-State Physics and Magnetism, KU Leuven, BE-3001 Leuven, Belgium

[⊥]Computer Science and Mathematics Division, Oak Ridge National Laboratory, Oak Ridge, TN 37831, USA

[#]Current address: Department of Physics, Pohang University of Science and Technology, Pohang 790-784, Republic of Korea

[@]Materials Science and Technology Division, Oak Ridge National Laboratory, Oak Ridge, TN 37831, USA

I. Wire-bundle characterization

Figure S1 shows a STM image of two bundles of YSi_2 wires of different widths together with a line profile taken at the location indicated by the black line. At this yttrium coverage (0.5±0.1 ML), the second silicide layer does not form a continuous structure over the whole length of the wire. Therefore we assume the height of the conducting wires to be that of a single YSi_2 layer, *i.e.* 0.5 ± 0.1 nm.

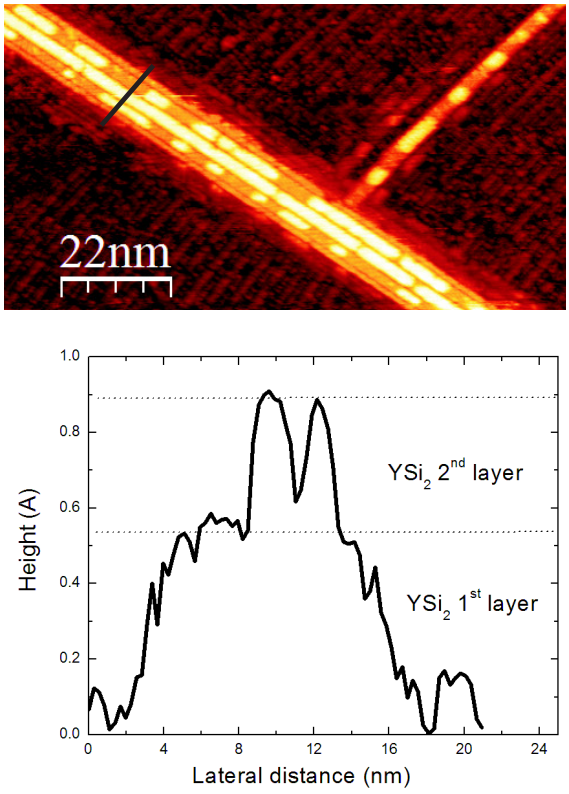

Figure S 1: Scanning probe characterization of YSi_2 bundles. Top panel shows a STM image with YSi_2 wires assembled in bundles. The bright protrusions are segments of second layer silicide. Tunneling parameters are -1.9 V and 0.05 nA. Bottom panel shows a line profile taken at the location indicated by the black line. The horizontal dotted lines are guides for the first and second silicide layer heights.[1]

Defect analysis from STM images

The number of defects in the wires is estimated from STM images of the uncapped wires. Figure S2 displays the frequency distribution of defects when adatoms and vacancies are considered. In

both cases the distributions peak at frequencies less then 10 nm per defect. This analysis includes both single wires as well as bundled wires. A STM image of a nanowire segment displaying several defects is shown in the inset of Figure S2.

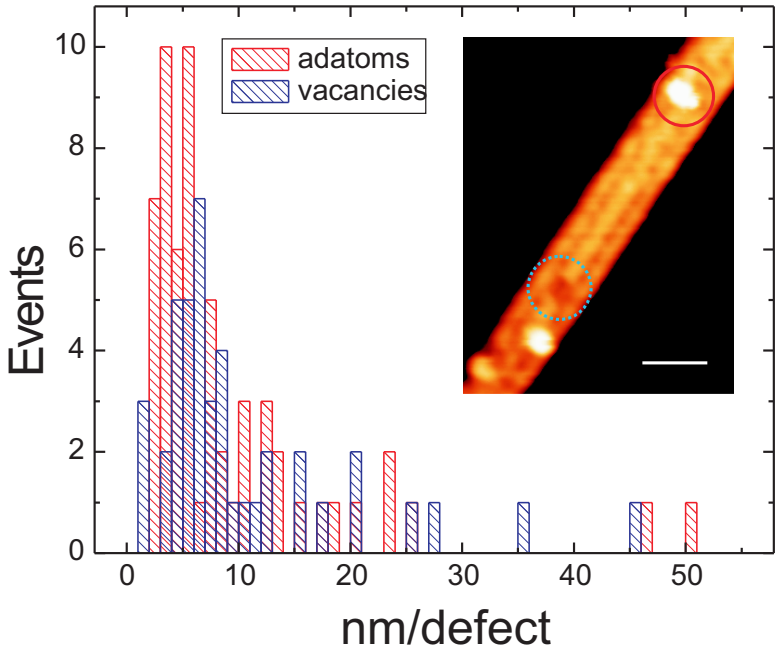

Figure S 2: Wire-defect analysis. Histogram indicating the defect frequency in the YSi_2 nanowires determined by defect counting from the STM images of the uncapped wires. Inset presents a STM image of a YSi_2 nanowire fragment displaying such defects. The solid (dotted) circle highlights an adatom (vacancy) defect site. Tunneling parameters are 0.05 nA, -1.7 V. Scale bar: 2 nm.

II. Control measurement: Platinum leads

To better understand and interpret the transport data obtained for the YSi_2 nanowires, we have independently determined the transport properties of the Pt leads. Pt wires having similar dimensions as the Pt leads used, were fabricated using electron beam induced deposition (EBID) of a precursor molecule, trimethyl(methylcyclopentadienyl)platinum(IV) (see Experimental section).[2] These Pt wires contain some fraction of organic material hence their electrical properties differ greatly from Pt wires fabricated from pure metal targets. Figure S3a, illustrates a SEM image of two Pt wires (cross section of 20 nm$\times$10 nm) connected by five square Pt electrodes. Figure S3b displays the

temperature dependence of the resistivity of such Pt wires. The measured resistivity at 300 K is 0.003 Ωcm and increases at lower temperatures. Similar values were reported by V. Gopal *et al.*[2]

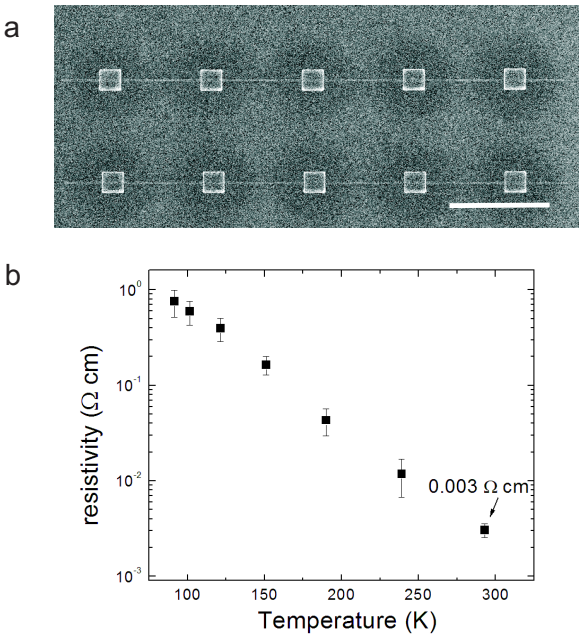

Figure S 3: Transport measurements of the Pt wire leads. (a) SEM image showing two Pt wires connected by 5 Pt electrodes (squares) (scale bar: 2 μm). (b) Temperature dependence of the resistivity of the Pt wires.

III. Control measurement: YSi_2 wetting layer

To further verify that the electronic transport detected when measuring the YSi_2 wire-samples occur through the wires, not the wetting layer, we have measured the conductivity of the wetting layer, *i.e.* the (2×7) reconstruction seen in the STM, using a similar measurement scheme. Square Pt electrodes were fabricated using the EBID technique (see Experimental section) onto the wetting layer to be contacted by the STM tips during the transport measurements. A SEM image of two rows of Pt electrodes is presented in the inset of Figure S4, panel a. $I - V$ characteristics were measured at several temperatures between 300 K to 80 K. Unlike the YSi_2 nanowires, the wetting layer measurements show nonlinear $I - V$ curves up to 300 K and exhibit a pronounced hysteresis at temperatures below 200 K (Figure S4a, b). The sheet conductivity of the wetting layer at room

temperature is determined to be $\sigma_S = 1.2 \times 10^{-8}\Omega^{-1}$, considering $C(4pp) = \pi\sigma_s/ln2$, where $C(4pp)$ is the measured four-probe conductance.[3] The measured conductivity is a few orders of magnitude lower than what we have measured for the nanowires, indicating that the electronic transport takes place indeed through the nanowire and not the substrate. Note also that the Schottky barrier, created at the interface between the substrate and the wire,[4] will electrically isolate the wires from the substrate at low voltages.

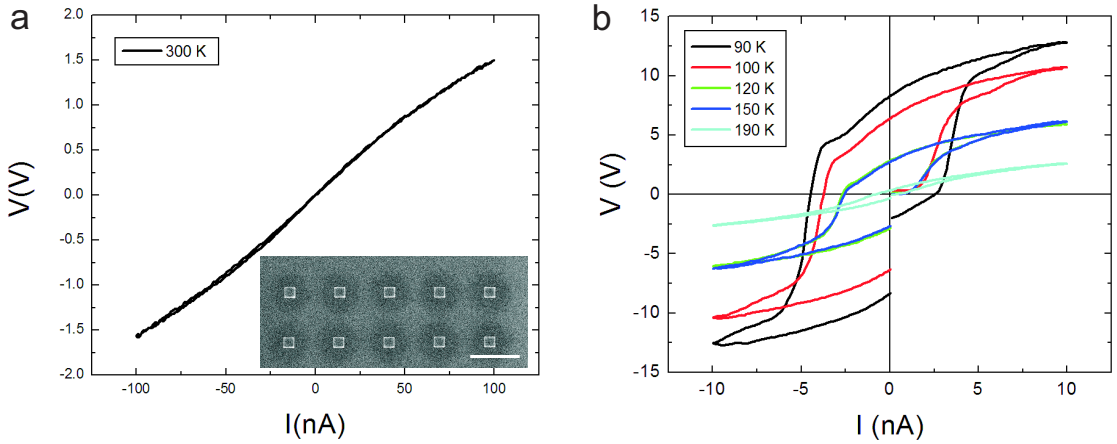

Figure S 4: Transport measurements for the YSi_2 wetting layer. (a) $I-V$ characteristic at 300 K. Inset displays an SEM image of two rows of Pt square contacts build over the wetting layer (scale bar: 2μm). (b) $I-V$characteristics show a pronounced hysteresis at low temperatures.

IV. YSi_2 bundle networks

$I-V$ characteristics measured for a device that included three YSi_2 wires are displayed in Figure S5. All the $I-V$ curves are fitted using the circuit model II from section VII with the fits being displayed as solid lines. The temperature dependence of the corrected wire resistance is displayed in Figure 3b in the main text.

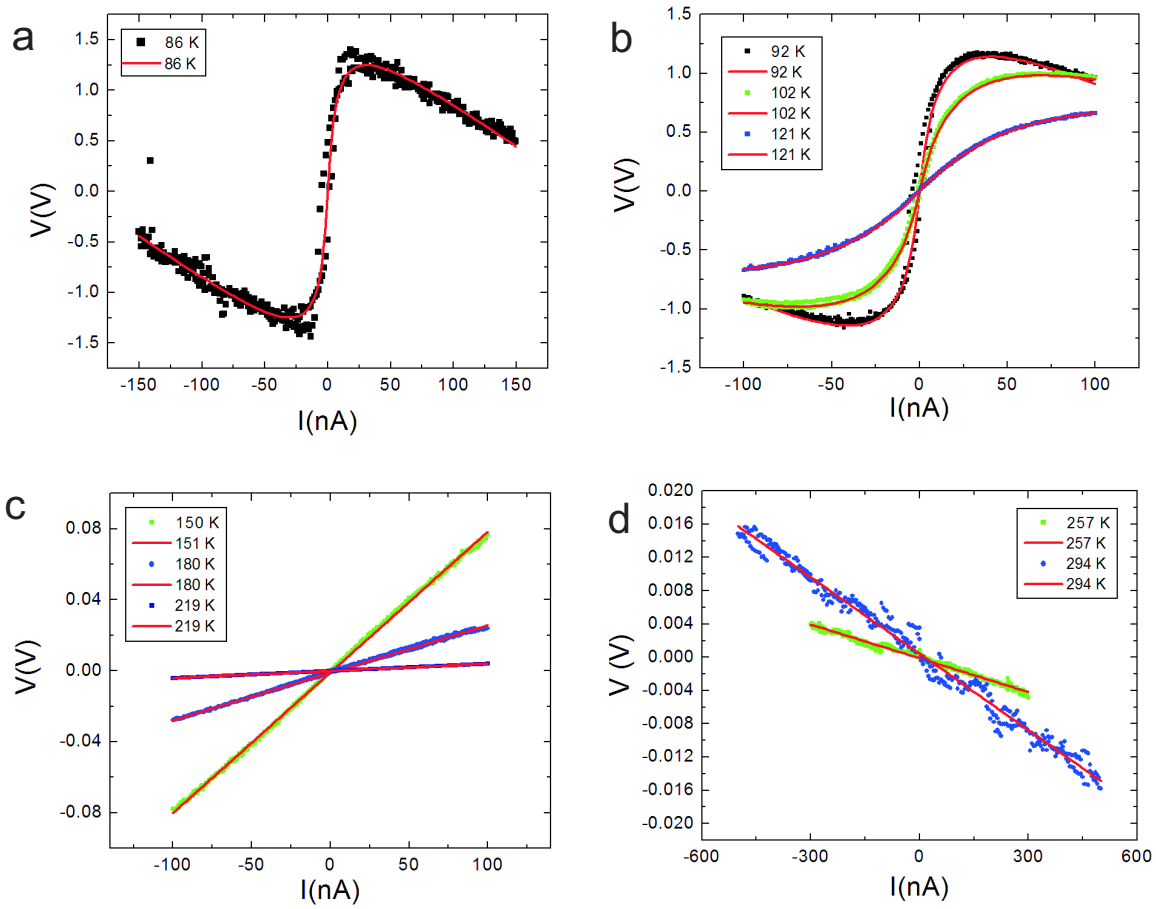

Figure S 5: YSi_2 wire network (wire 14). (a) to (d), $I - V$ characteristics of wire 14 device that consists of a network of three YSi_2 nanowires. The solid lines are fits to the data using the circuit model II (see section VII).

V. Polaron hopping in a single wire

The current through a quasi-one-dimensional disordered conductor as a function of temperature and voltage has been derived by Osipov et al.[5] The derivation is based on the probability of phonon-assisted hopping between neighboring impurity sites, computed using the Fermi golden rule. At elevated temperatures, the absorption of a phonon to raise the electron energy by E to an excited impurity state leads to a Boltzmann factor $\exp(-E/kT)$ in the transition rate, while tunneling through the barrier potential between two impurity sites leads to an exponential factor $\exp[-S(E)]$, where $S(E)$ is expressed[5] in terms of the polaron shift I_p (the energy lowering of the defect levels resulting from the local bond deformation or restructuring upon electron capture), the voltage drop

between the two impurity sites V_{12} (contained within the barrier potential $U(z)$),and the phonon frequency ω,

$$S(E) = \frac{I_p}{2\hbar\omega} \int dz \sqrt{2[U(z) - E]}, \tag{1}$$

where $U(z)$ is the barrier potential between the impurities.

For the limit of $V_{12} \ll I_p$, the transition rate between two neighboring impurity sites is evaluated to yield,[5]

$$\nu_{12} \propto \exp\left[-\frac{2I_p}{\hbar\omega}\tanh(\hbar\omega/4kT) + \frac{|eV_{12}|}{2kT}\right]. \tag{2}$$

Here we keep an additional term in V_{12} compared to Ref. 5 in order to fit the experimental I-V curves to higher voltages.

Now we consider a nanowire containing a sequence of impurity centers, labeled by 1, 2, ..., i, ..., N. The transition rate between two neighboring centers, $i-1$ and i, is

$$\nu_{i-1,i} = C_{i-1,i} \exp\left[-\frac{2I_{i-1,i}}{\hbar\omega}\tanh(\hbar\omega/4kT) + \frac{|eV_{i-1,i}|}{2kT}\right], \tag{3}$$

where $C_{i-1,i}$ is a prefactor independent of temperature and voltage. The current is

$$I(V,T) = e[f_{i-1} - f_i]\nu_{i-1,i} = e^2 V_{i-1,i} D_{\rm imp} \nu_{i-1,i}, \tag{4}$$

where we have assumed $\nu_{i-1,i} = \nu_{i,i-1}$ and $f_{i-1} - f_i = D_{\rm imp} e V_{i-1,i}$ which defines an effective impurity state density of states $D_{\rm imp}$. This is simply a resistor in series problem and the steady state solution is,

$$I(V,T) = \frac{e^2 V D_{\rm imp}}{\sum_i \nu_{i-1,i}^{-1}}. \tag{5}$$

If we neglect the fluctuations from impurity to impurity, and set the values $I_{i-1,i} = I_p$, and $V_{i-1,i} = V/n$ where n is the number of impurities in the wire, we find,

$$I(V,T) = \frac{e^2 V D_{\rm imp} \nu}{n}, \tag{6}$$

where ν is the polaron hopping frequency, which using eq 3 leads to,

$$I(V,T) = J_0 V \exp\left[-\frac{2I_p}{\hbar\omega}\tanh(\hbar\omega/4kT) + \frac{|eV|}{2nkT}\right]. \tag{7}$$

with $J_0 = e^2 D_{\rm imp} C/n$.

VI. Polarization-induced resistance, model I

Suppose there are two parallel wires, one with a small resistance and one with a large resistance due to a single, strong scattering center. As the current is increased, the wire with the large resistance will build up a local charge proportional to the current. The Coulomb field from this charge buildup may create a scattering potential in the other wire. For sufficiently strong coupling this can shut off transport in the other wire.

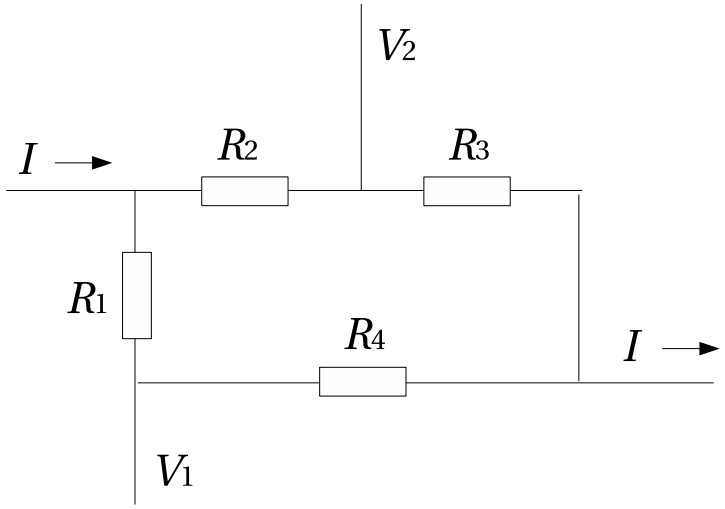

Figure S 6: Circuit model for the four-probe measurement with two nanowires. R_1 is the resistance of the Pt lead connected to the first voltage probe. R_2 and R_3 are resistances of the sections of the first nanowire. R_4 is the resistance of the second nanowire.

Suppose two nanowires are in parallel in the four-probe measurement, as shown in Figure S6, where the two current leads are indicated by I (with the arrows indicating the current direction), and the two voltage leads are indicated by V_1 and V_2, respectively. R_2 and R_3 represent the wire with the small (zero current) resistance and R_4 is the wire with the large resistance. Therefore when $I = 0$, $R_4 \gg R_2$ and $R_4 \gg R_3$. As the current is increased, the inhomogeneity in the second wire causes the charge to build up, whose Coulomb field in turn changes the resistances R_2 and R_3. If R_2 has a strong coupling to R_4 we should see a nonlinear increase of the resistance as a function of the voltage. However, if R_2 couples weakly to R_4 but R_3 couples strongly to R_4, then a decrease of the measured voltage $V = V_2 - V_1$ as a function of the increasing current can occur. From the circuit model in Figure S6, we find,

$$V = V_2 - V_1 = \frac{R_2 R_4 - R_1 R_3}{R_1 + R_2 + R_3 + R_4} I. \tag{8}$$

If we assume that R_2 does not change with the voltage on R_4 but R_3 is proportional to it, then

$$R_3 = \lambda |V_4| = \lambda |I| \frac{(R_2 + R_3) R_4}{R_1 + R_2 + R_3 + R_4}, \tag{9}$$

where V_4 is the voltage drop on R_4 and λ is the coupling constant between R_3 and R_4. Solving for R_3 and keeping only the positive root, we find,

$$R_3 = \frac{1}{2}[(\lambda|I| - 1)R_4 - R_1 - R_2] + \sqrt{\frac{1}{4}[(\lambda|I| - 1)R_4 - R_1 - R_2]^2 + \lambda|I|R_2 R_4}. \tag{10}$$

If $\lambda|I| \gg 1$ then,

$$R_3 \approx (\lambda|I| - 1)R_4. \tag{11}$$

If $\lambda|I| \ll 1$ then,

$$R_3 \approx \lambda|I|R_2. \tag{12}$$

Interpolating between these two limits, the voltage drop depends nonlinearly on the current,

$$V \approx \frac{aR_2 - \lambda|I|R_1}{a + \lambda|I|} I, \tag{13}$$

where a is a constant for the interpolation.

At small currents, the measured resistance is R_2. At large currents, the measured resistance is $-R_1$. This can be further written as

$$V = \frac{B - |I|}{C + |I|} R_1 I, \tag{14}$$

which we use to fit the experiment. Here $B = aR_2/\lambda R_1$ and $C = a/\lambda$. Alternatively, if R_2 is proportional to the voltage drop V_4 on resistor R_4 but R_3 is independent,

$$R_2 = \lambda|V_4| = \lambda_2|I|\frac{(R_2 + R_3)R_4}{R_1 + R_2 + R_3 + R_4} \tag{15}$$

then we find the opposite result, where the resistance is negative for small current and positive for large current. This is the opposite of what is seen experimentally at low temperatures (see Figure S4 (a)). Thus we conclude that R_2 does not vary with the current at low temperatures.

VII. Polarization-induced resistance, model II

In Figure S7 we show a more complex circuit made of three nanowires. In this case the measured voltage drop is,

$$V = V_2 - V_1 = \left\{ R_3 - \frac{(R_1 + R_3)[(R_3 + R_4)(R_2 + R_5) + R_3R_4]}{(R_1 + R_3 + R_6)(R_2 + R_4 + R_5) + R_4(R_2 + R_5)} \right\} I. \tag{16}$$

If $R_4 \gg R_1 + R_2 + R_3$, then,

$$V \approx \frac{R_3R_6 - R_1(R_2 + R_5)}{R_1 + R_2 + R_3 + R_5 + R_6} I. \tag{17}$$

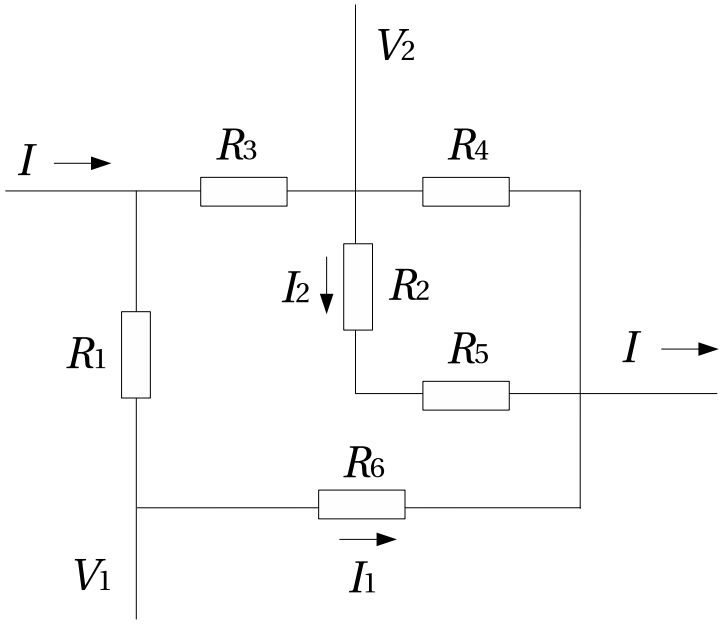

Figure S 7: Circuit model for the four-probe measurement with three nanowires. R_1, R_2 are the resistances of the segments of the Pt leads connected to the voltage probes. R_3 and R_4 are resistances of the sections of the first nanowire. R_5 is the resistance of the second nanowire, and R_6 is the resistance of the third wire.

Consider the Coulomb field from R_4 and R_6 on R_5. If we assumed that the resistance R_5 is,

$$R_5 = \lambda_1 |I_1| R_6 + \lambda_2 |I - I_1 - I_2| R_4, \tag{18}$$

then,

$$x = R_2 + \lambda_2 |I| R_4 + \frac{(\lambda_1 R_6 - \lambda_2 R_4)(R_3 + R_4)x + \lambda_1 R_3 R_4 R_6 - \lambda_2 (R_1 + R_3 + R_6) R_4^2}{(R_1 + R_3 + R_4 + R_6)x + R_4 (R_1 + R_3 + R_6)} |I|, \tag{19}$$

where $x = R_2 + R_5$. Assuming that $R_4 \gg R_1 + R_2 + R_3$, the approximate solution is,

$$R_5 \approx \lambda |I| \frac{R_4 R_6}{R_4 + R_6}, \tag{20}$$

where $\lambda = \lambda_1 + \lambda_2$.We have,

$$V \approx \frac{(R_3R_6 - R_1R_2)(R_4 + R_6) - \lambda|I|R_1R_4R_6}{(R_1 + R_2 + R_3 + R_6)(R_4 + R_6) + \lambda|I|R_4R_6} I. \tag{21}$$

This I-V curve is also the form of eq 14, with both B and C proportional to $1/\lambda$, similar to model I, but the fitted ratio B/C is related to the resistances,

$$\frac{R_3R_6 - R_1R_2}{R_1 + R_2 + R_3 + R_6} = \frac{B}{C} R_1. \tag{22}$$

To further simplify the above expression, we assume an average single wire resistance $R_{\rm WIRE} = (R_3 + R_6)/2 \approx \sqrt{R_3R_6}$, and an average contact resistance $R_C = (R_1 + R_2)/2 \approx \sqrt{R_1R_2}$, neglecting the difference between the arithmetic and geometric averages, where R_C is assumed to be the resistance due to the Pt wires. We finally obtain,

$$R_{\rm WIRE} \approx 2\frac{B}{C} R_1 + R_C. \tag{23}$$

For data measured below 150 K, we can fit with three parameters B, C, and R_1. But for data measured above 150 K only the slope of the I-V curve can be reliably determined, which gives us $(B/C)R_1$. At high temperatures $(B/C)R_1$ becomes negative, which gives a lower bound for the values of R_C. If we assume that R_C follows the same temperature dependence as the Pt wires, whose resistivity is measured separately, then the only fitting parameter needed to determine R_C is the length of the Pt wire. We can fit this length by requiring that the high temperature part of the data all fall on an Arrhenius curve. Fitting to wires 14 and 15 yielded effective lengths of 1.5 μm and 2.25 μm, respectively, for the Pt wire lengths.

We have used two different circuit models to derive a simple nonlinear I-V formula, eq 14. We assert that eq 14 can be generally assumed for an interacting network of nanowires mediated by a Coulomb field through the substrate. Of course the particular meanings of the fitting parameters R_1, B and C should depend on the details of the circuit model. While a four-probe setup can

eliminate the problem of contact resistance for single wires, for a wire network one would need two additional probes for each wire branch to completely eliminate the problem of contact resistance. Nonetheless, with the help of our circuit model, we are able to take full advantage of the four-probe measurement setup and reduce the final number of fitting parameters to two or three (see eq 14 and eq 23 or eqs 2 and 3 of the main document). The negative resistivity observed at high temperatures for some of the samples is now easily explained by eq 23: if the wire resistance R_{WIRE} is less than the contact resistance R_C, then B/C becomes negative.

VIII. Temperature dependence of the inter-wire coupling

The temperature dependence of the inter-wire coupling arises from the contribution to the polaron activation energy E_a from neighboring wires due to the coupling through the substrate. According to Vannikov et al,[6] this contribution is,

$$\Delta E_a = \frac{e^2}{4\pi\epsilon_0}\left(\frac{1}{\epsilon_\infty} - \frac{1}{\epsilon(\omega_p)}\right)\left(\frac{1}{a_0} - \frac{1}{\rho}\right), \tag{24}$$

where ϵ_∞ is the optical dielectric constant for the medium,$\epsilon(\omega_p)$ is the dielectric constant at the polaron hopping frequency $\omega_p = 2\pi\nu$, a_0 is the separation between the nanowires,and ρ is the average distance between the impurities in the nanowire. The dielectric constant $\epsilon(\omega_p)$ can be approximated in a simple form,[7]

$$\epsilon(\omega_p) = \epsilon_\infty\left(1 + \frac{\Omega_p^2}{\omega_{TO}^2 - \omega_p^2}\right), \tag{25}$$

where ω_{TO} is the transverse optical (TO) phonon mode, Ω_p^2 is a parameter that relates to the oscillator strength of the TO phonon,and we assumed a single mode for simplicity. At low temperatures when the polaron hopping frequency ω_p is small, $\epsilon(\omega_p) > \epsilon_\infty$, therefore $\Delta E_a > 0$ and the polaron activation energy is increased by inter-wire coupling through the medium. At a certain temperature T_c, when $\omega_p \approx \omega_{TO}$, the dielectric constant$\epsilon(\omega_p)$ encounters a resonance. Somewhat above

this temperature ΔE_a vanishes, the inter-wire coupling becomes zero, and the polaron activation energy returns to the value for a single wire. Thus near T_c we should observe two effects, the disappearance of the inter-wire coupling, and a discontinuity of the conductance as a function of temperature. From experimental data, this happens at about $T_c \approx 150$ K. Although we cannot measure the polaron hopping frequency directly, we can estimate it from the measured single wire resistance $R(T)$ by applying eq (6) at the critical temperature, T_c,

$$\omega_{TO} \approx \frac{2\pi n}{e^2 R(T_g) D_{\rm imp}}, \tag{26}$$

where we recall that n is the number of impurities in the wire. This relationship may be used to check the validity of the polaron model.

IX. Density functional theory calculations of wire defects

To assess possible values for the impurity DOS we performed electronic structure calculations of defective wires. We employed density functional theory and the plane wave projector augmented wave method[8–11] within the local density approximation.[12] We used supercells containing a slab with nine layers of Si atoms depth and sufficient width to study independent $5a_0$ wires. All atomic positions were fully relaxed, except for the lowest plane of Si atoms. The rear surface was passivated with hydrogen atoms. Other parameters were identical to our earlier studies.[13] We studied the electronic structure of a supercell containing 8 repeats of the $5a_0$ wire, with a single Y vacancy introduced in the centre of the wire. Our final supercell contained 1191 atoms, yielding a periodic vacancy-vacancy separation of 3.055 nm. Brillouin zone integration used a $3\times2\times1$ gamma-point centred k-point grid.

To determine the impurity DOS we compared the wavefunctions and bandstructure within a 1eV window of the Fermi energy with those of a perfect wire (vacancy free) supercell. To clearly identify impurity states, we computed the integrated charge of each state with distance from the vacancy site. Using the criteria that 60% of the integrated charge must be within 1nm of the

vacancy, we identified two impurity states. Visualization of these states verified their vacancy-related character. The most localized state has $\approx 65\%$ of its charge within 1nm of the vacancy site. Modest variations of these criteria consistently identify one or two impurity states. Weaker criteria consistently identified less-localized non-impurity states already present in the perfect wire supercell. We therefore conclude that $D_{\mathrm{imp}} \approx 1$ eV^{-1} for this wire. Bond counting arguments and the similarity of local structures suggests that other common defects are likely to yield DOS similar values.

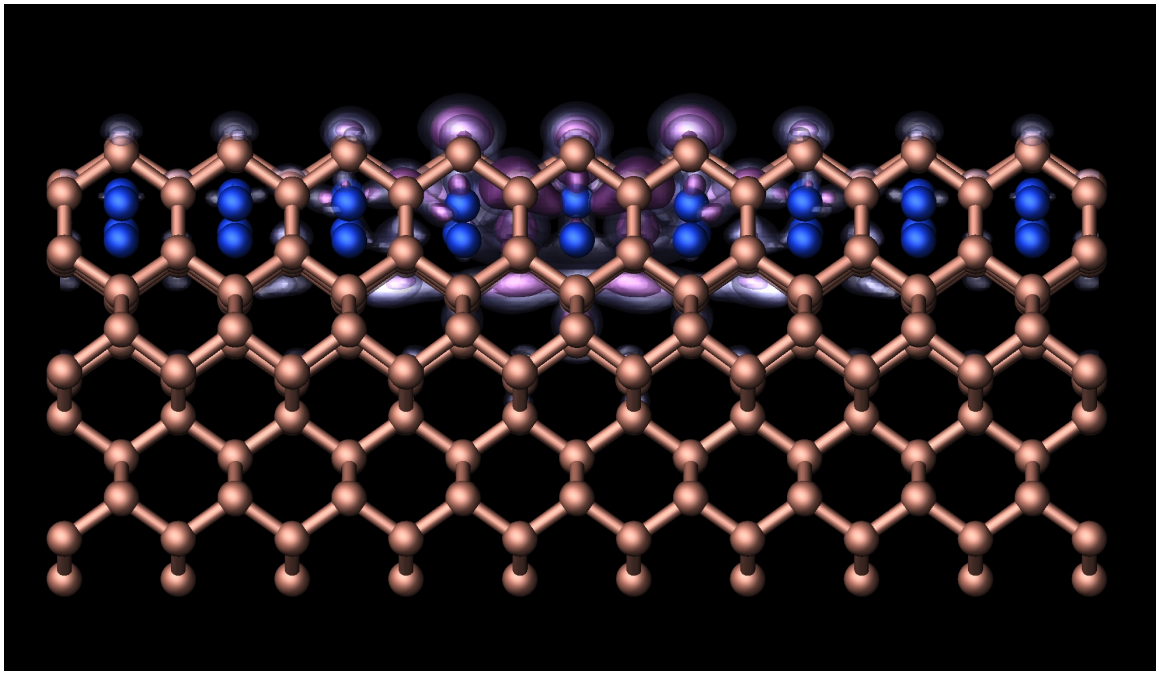

Figure S 8: Visualization of the localized vacancy state in defective YSi_2 wires. The clouds represent the isosurfaces of the square of the most localized state. The vacancy (missing blue Y atom) is "behind" the lower visible Y in the centre of the plot.

References

(1) Liu, B. Z.; Nogami, J. *J. Appl. Phys.* **2003**, *93*, 593–599.

(2) Gopal, V.; Radmilovic, V. R.; Daraio, C.; Jin, S.; Yang, P.; Stach, E. A. *Nano Lett.* **2004**, *4*, 2059–2063.

(3) Wells, J. W.; Kallehauge, J. F.; Hansen, T. M.; Hofmann, P. *Phys. Rev. Lett.* **2006**, *97*, 206803–1–4.

(4) Huang, W. *Microelectr. Eng* **2008**, *85*, 131–135.

(5) Osipov, V. V.; Foygel, M.; Stewart, D. R.; Williams, R. S. *J. Phys.: Condens. Matter* **2004**, *16*, 5705–5712.

(6) Vannikov, A. V.; Kryukov, A. Y.; Tyurin, A. G.; Zhuravleva, T. S. *physica status solidi (a)* **1989**, *115*, K47–K51.

(7) Evans, E.; Mills, D. L. *Phys. Rev. B* **1973**, *8*, 4004–4018.

(8) Kresse, G.; Hafner, J. *Phys. Rev. B* **1993**, *47*, 558–561.

(9) Kresse, G.; Hafner, J. *Phys. Rev. B* **1994**, *49*, 14251–14269.

(10) Blöchl, P. E. *Phys. Rev. B* **1994**, *50*, 17953–17979.

(11) Kresse, G.; Joubert, J. *Phys. Rev. B* **1999**, *59*, 1758–1775.

(12) Perdew, J. P.; Zunger, A. *Phys. Rev. B* **1981**, *23*, 5048–5079.

(13) Iancu, V.; Kent, P. R. C.; Hus, S.; Hu, H.; Weitering, H. H. *J. Phys.: Condens. Matter* **2013**, *25*, 014011–1–12.